Chemistry & Biology, Vol. 11, 475–485, April, 2004, ©2004 Elsevier Science Ltd. All rights reserved. DOI 10.1016/j.chembiol.2004.03.019

Novel Real-Time Sensors to Quantitatively Assess In Vivo Inositol 1,4,5-Trisphosphate Production in Intact Cells

Kenji Sugimoto,[1] Motohiro Nishida,[2] Masami Otsuka,[4] Keisuke Makino,[1] Katsutoshi Ohkubo,[1] Yasuo Mori,[2,3,5,*] and Takashi Morii[1,6]

[1]Institute of Advanced Energy
Kyoto University
Uji, Kyoto 611-0011
[2]Center for Integrative Bioscience
Okazaki National Research Institutes
[3]School of Life Science
The Graduate University for Advanced Studies
Okazaki 444-8585
[4]Faculty of Bioorganic Medical Chemistry
Graduate School of Pharmaceutical Sciences
Kumamoto University
Kumamoto 862-0973
[5]Laboratory of Molecular Biology
Department of Synthetic Chemistry and Biological Chemistry
Graduate School of Engineering
Kyoto University
Kyoto 615-8510
[6]PRESTO, JST
Uji, Kyoto 611-0011
Japan

Summary

Real-time observation of messenger molecules in individual intact cells is essential for physiological studies of signaling mechanisms. We have developed a novel inositol 1,4,5-trisphosphate (IP_3) sensor based on the pleckstrin homology (PH) domain from phospholipase C (PLC) δ. The environmentally sensitive fluorophore 6-bromoacetyl-2-dimethyl-aminonaphtalene was conjugated to the genetically introduced cysteine at the mouth of the IP_3 binding pocket for enhanced IP_3 selectivity and for rapid and direct visualization of intracellular $IP_3 \geq 0.5$ μM as fluorescence emission decreased. The probe, tagged with arginine-rich sequences for efficient translocation into various cell types, revealed a major contribution of Ca^{2+} influx to PLC-mediated IP_3 production that boosts Ca^{2+} release from endoplasmic reticulum. Thus, our IP_3 probe was extremely effective to quantitatively assess real-time physiological IP_3 production via those pathways formed only in the intact cellular configuration.

Introduction

Phospholipase C (PLC) plays a central role in phosphatidyl inositol response, generating inositol 1,4,5-trisphosphate (IP_3) and diacylglycerol through hydrolysis of phosphatidylinositol-4,5-bisphosphate (PIP_2) in response to activation of plasma membrane receptors for neurotransmitters, hormones, autacoids, Ca^{2+}, antigens, and growth factors. In various types of cells, IP_3 production leads to biphasic increase in intracellular Ca^{2+} concentration ($[Ca^{2+}]_i$), which controls diverse cellular processes [1, 2]. The first phase of $[Ca^{2+}]_i$ increase reflects Ca^{2+} release from intracellular Ca^{2+} stores, endoplasmic reticulum (ER), via opening of IP_3 receptors (IP_3Rs) by IP_3 [2–4], while the sustained phase is due to influx of Ca^{2+} from the extracellular space through channels in the plasma membrane that have variously been referred to as receptor-activated Ca^{2+} channels [1, 5, 6]. IP_3 is involved in activation of these ion channels through IP_3-induced Ca^{2+} release/store depletion via IP_3R or direct action of IP_3 itself as Ca^{2+}, inositol 1,3,4,5-tetraphosphate (IP_4), and arachidonic acid metabolites [2, 7–9]. Thus, IP_3 plays a key role in the signaling cascades to link extracellular messengers to intracellular Ca^{2+} mobilization.

The conventional HPLC and capillary electrophoretic analyses [10, 11] and the assay based upon competition between generated IP_3 and radiolabeled IP_3 for binding to the binding protein [12] have been previously employed to assess metabolism of IP_3. These methods require destruction of cells. Recently, for real-time detection of temporal and spatial dynamics of inositol lipids in intact cells, green fluorescent proteins (GFP) fused to the protein motifs that mediate the interactions with the phosphoinositides have been invented [13]. Hirose et al. [14] have demonstrated agonist-induced translocation of GFP-tagged PH domain of PLCδ, which was discussed to be mainly due to PIP_2 metabolization and subsequent increase in intracellular IP_3 concentration ($[IP_3]_i$). Despite the usefulness of the genetically encoded GFP-based phosphoinositide probes, several drawbacks that may complicate interpretations have been also pointed out [13]. The probes can bind both inositol lipids and soluble phosphoinositides [14, 15]. Furthermore, stable overexpression of the probes can significantly change the molecular geography by sequestration of inositol lipids and might exert inhibitory effects on various lipid-dependent cellular functions [13]. In an attempt to develop a biosensor that specifically detects $[IP_3]_i$ changes, we have combined a site-directed mutagenesis/recombinant expression technique with chemical modification with fluorophore. The results demonstrate efficient cellular incorporation of the newly developed IP_3 probe and selective detection of IP_3 by the probe in various types of intact cells. Use of the probe enabled a real-time detection of Ca^{2+} influx-enhanced IP_3 production, which can be only assessed in the intact cellular configuration.

Results

Properties of the Fluorophore-Conjugated PH Domain as an IP_3 Sensor and Its Genetic Manipulation for Improved Cellular Incorporation

We have previously described a basic strategy for designing optical direct IP_3 sensors with higher selectivity

*Correspondence: mori@sbchem.kyoto-u.ac.jp

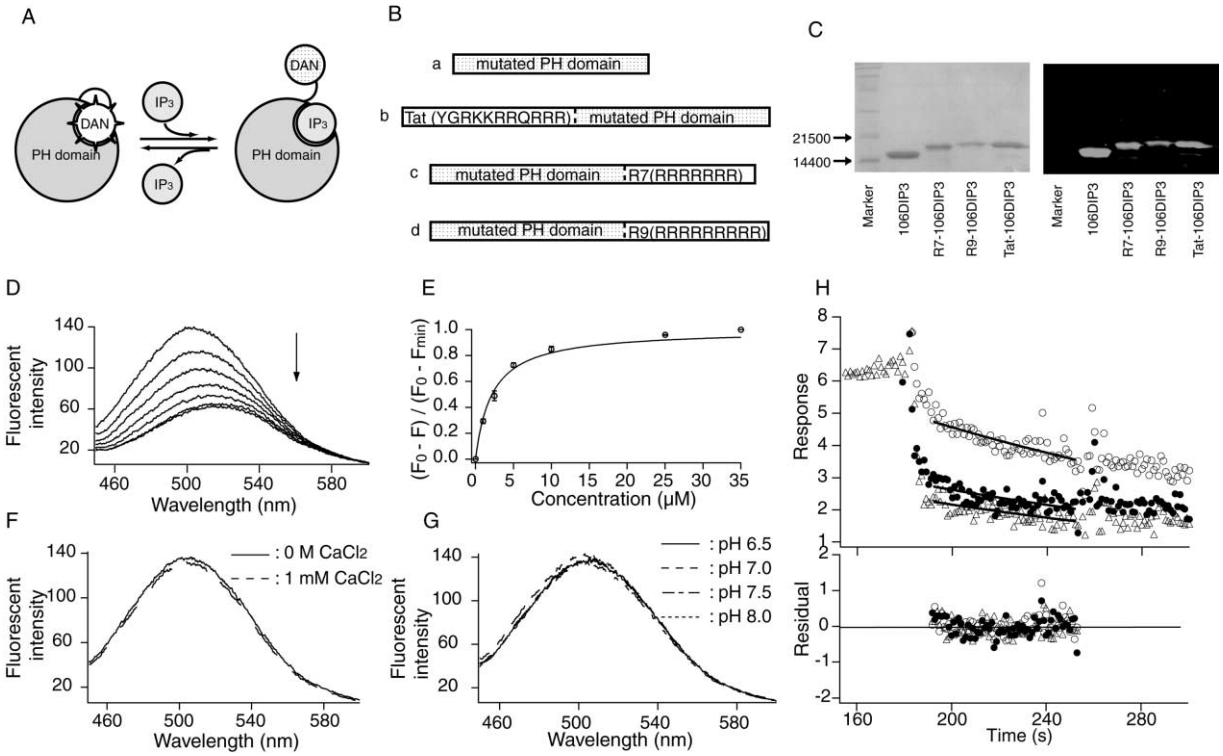

Figure 1. In Vitro Properties of the IP_3 Sensor R9-106DIP3

(A) A schematic representation shows the fluorescence change of R9-106DIP3 associated with IP_3 binding. (B) A schematic diagram depicting (a) PLCδ_1 PH domain substituted Cys106 for Asn106 and PLCδ_1 PH domain substituted Cys106 for Asn106 fused with (b) Tat (Tat-106DIP3), (c) R7 (R7-106DIP3), or (d) R9 (R9-106DIP3) peptide. The meshed portions indicate PLCδ_1 PH domain substituted Cys106 for Asn106.

(C) The IP_3 sensors visualized by CBB staining (left) or by transilluminator irradiation (right) after 15% SDS-polyacrylamide electrophoresis.

(D) Emission spectra of the R9-106DIP3 with increasing amounts of IP_3. An arrow indicates the decrease in the spectral intensity upon addition of IP_3 (0−35 μM).

(E) Binding isotherm for R9-106DIP3 obtained by fluorescent titrations with IP_3. The binding ratio [(Fo-F)/(Fo-F_{min})] was plotted against the IP_3 concentration.

(F and G) The fluorescence emission spectra of R9-106DIP3 independent of the changes in Ca^{2+} concentration (F) and pH (G) of the solution.

(H) Dissociation speed (k_{off}) determined by the surface plasmon resonance measurement. Shown is a sensorgram showing the dissociation of 106DIP3-IP_3 complex (top) with 200 nM (open circles), 100 nM (filled circles), and 50 nM (open triangles) 106DIP3. Solid lines represent theoretical fitting curves for dissociation, and deviations are shown in the bottom column. Dissociation speed (k_{off}) is 4.24 ± 0.45, 4.25 ± 0.76, and 4.32 ± 0.89 ($\times 10^{-3}$) s^{-1} at 106DIP3 concentrations of 50, 100, and 200 nM, respectively. Association speed (k_{on}) obtained using $Kd = k_{off}/k_{on}$ is 1.92, 1.92, and 1.95 ($\times 10^3$) $M^{-1}s^{-1}$ at 106DIP3 concentrations of 50, 100, and 200 nM, respectively.

than the original PLCδ-PH [16]. In the sensor protein constructs, single cysteine (Cys) mutations were first introduced at residues such as aspargine (Asn) 106, whose β carbons are located 8–9.7 Å away from the C2 carbon of bound IP_3. The fluorophores were then conjugated to the residues so that they would snugly fit in the binding pocket to prevent semispecific ligand binding (Figure 1A). The fluorophore 6-bromoacetyl-2-dimethyl-aminonaphtalene (DAN) was conjugated at Asn 106 replaced with Cys in the PLCδ-PH-based IP_3 sensor.

We carried out an additional manipulation of the sensor protein to optimize the structure of the probe for in vivo usage, since the intact probe showed no significant translocation across plasma membrane and incorporation into cells. Several arginine (Arg)-rich polypeptides, including HIV-1 Tat-(48-60) and Antennapedia-(43-58), have been previously reported for their ability to translocate proteins across plasma membrane [17–31]. The PLCδ-PH protein was fused to these peptide sequences to produce the sensor derivatives, as shown in Figure 1B. Figures 1D–1H depict in vitro optical behavior of sensor R9-106DIP3, which is the Arg $(R)_9$-tagged PH domain conjugated with DAN at the cysteine residue 106. Decrease of emission intensity of R9-106DIP3 (formerly referred to as R9-PHIP_3-D106 [32]) through IP_3 binding in response to increase of IP_3 concentration can be theoretically fitted to the following calibration equation (Figures 1D and 1E):

$$\Delta F = \Delta F_{max} \{[IP_3]/(Kd + [IP_3])\}, \quad (1)$$

in which the Kd value is 2.21 μM. The data show an in vitro dynamic range of the R9-106DIP3 probe 0.5 to 25 μM. We examined the in vitro effects of several important cellular factors that might affect the IP_3-sensing ability of the R9-106DIP3 probe. Changing the $CaCl_2$ concentration (0–1 mM) or pH (6.5–8) failed to affect emission behavior of R9-106DIP3 in vitro (Figures 1F and 1G). Affinity of IP_3 binding of R9-106DIP3 was slightly

Table 1. Binding Affinity of the IP_3 Sensors with Inositol Phosphate Derivatives

pH	Ca^{2+} (μM)	Mg^{2+} (mM)	ATP (mM)	K^+ (mM)[a]	Kd (μM)	P[b]
6.5	0	—	—	—	4.91 ± 0.91	**
7.0	0	—	—	—	2.21 ± 0.17	
7.0	0.1	—	—	—	2.86 ± 0.24	*
7.0	1	—	—	—	2.97 ± 0.38	*
7.0	10	—	—	—	2.44 ± 0.17	NS
7.0	1000	—	—	—	3.33 ± 0.43	*
7.0	0	5	1	—	3.89 ± 0.48	**
7.0	0	—	—	150	5.27 ± 0.12	***
7.5	0	—	—	—	1.90 ± 0.23	NS
8.0	0	—	—	—	1.17 ± 0.15	**

NS, not significant; *, $p < 0.05$; **, $p < 0.01$; ***, $p < 0.001$.
[a] 50 mM NaCl was replaced with 150 mM KCl.
[b] Significance from control (pH 7.0, without K^+, Ca^{2+}, Mg^{2+}, or ATP).

diminished by addition of Ca^{2+} alone or Mg^{2+} plus ATP, by replacement of Na^+ with K^+, and by pH decrease (Table 1). As already demonstrated in the previous paper, the conjugation with DAN created a sensing selectivity to IP_3 over other inositol phosphates (Table 2) [16]. Among the tested inositol phosphates, inositol hexaphosphate showed a *Kd* comparable to that of IP_3. Furthermore, PIP_2 binding assay using the PIP_2 resin demonstrated that the original PLCδ PH domain bound efficiently to the PIP_2 resin and was eluted by 50 μM IP_3, whereas R9-106DIP3 showed no significant binding to the PIP_2 resin (see Supplemental Figure S1 available with this article online). Furthermore, Mg^{2+} and ATP failed to confer affinity to PIP_2 on R9-106DIP3, supporting a potential of R9-106DIP3 for selective detection of IP_3 in physiological milieu. Importantly, the dissociation speed evaluated from the binding experiments using the surface plasmon resonance technique (Figure 1H) and the above *Kd* value determined by the optical measurement reveal an association speed indicative of rapid incorporation of IP_3 by 106DIP3 (see legend to Figure 1H). The data implied a potential of the probe R9-106DIP3 as an effecient in vivo IP_3 sensor.

The untagged sensor probe showed very poor translocation activity across plasma membrane into cells in observation under confocal microscope (Figure 2A). Strikingly, the arginine-rich sequence-tagged derivatives displayed greatly enhanced intracelular incorporation at 37°C: more than half of chicken DT40 B cells incorporated the arginine-rich sequence-tagged sensors, such as TAT tagged (57% incorporation), R_7-heptapeptide-tagged sensor proteins (61%), and R_9-nonapeptide-tagged R9-106DIP3 (61%), in the presence of the nonionic sulfactant polyol detergent Pluronic F127, which has been routinely used to load ion indicators such as fura-2 and fluo-3 (Figures 2B–2D). Costaining experiments using organelle-specific probes revealed a diffusive distribution of the IP_3 sensor R9-106FIP3 conjugated with fluorescein throughout the cells (Figures 2E–2G), in contrast with PLCδ_1 PH domain-GFP fusion protein highly localized at the plasma membrane of unstimulated cells [13, 14].

Similar distribution was observed in other types of cells, such as CHO-K1 cells or human embryonic kidney (HEK) cells (data not shown). Since the three IP_3 sensor derivatives behaved similarly in intracellular incorporation, we focused on arginine nonapeptide-tagged R9-106DIP3 in the following experiments.

Table 2. Effects of Ca^{2+}, Mg^{2+}, ATP, pH Changes, and Complete Exchange of Na^+ with K^+ on *Kd* for Complex Formation of R9-106DIP3 with IP_3

Inositol Phosphate	K_d (μM)	S[a]
IP_1	>>100	>>45
Ins(1,4,5)P_3	2.21 ± 0.17	1
Ins(1,3,4)P_3	440 ± 16.3	200
L-Ins(1,4,5)P_3	28.18 ± 0.20	12.8
Ins(1,3,4,5)P	63.68 ± 6.33	29.8
IP_6	4.03 ± 0.65	1.8
PIP_2	>>10[b]	>>4.5

K_d for inositol phosphate binding of the IP3 sensor 106DIP3 was analyzed by fluorescence measurement.
[a] S represents the ration to the dissociation constant for Ins(1,4,5)P_3.
[b] K_d of binding to R9-106DIP3.

In Vivo Behavior of the IP_3 Probe

In assessing the efficiency of R9-106DIP3 as an in vivo IP_3 sensor, we recorded and analyzed changes of fluorescence images of the cells with a video image analysis system at an emission wavelength of 510 nm (bandwidth, 20 nm) by exciting at 380 nm (bandwidth, 11 nm) at room temperature. After 10 min incubation of DT40 chicken B cells with R9-106DIP3, IP_3-induced emission change of the probe in the cellular environment was observed by permeabilizing the cells with β-escin under controlled IP_3 concentration (Figure 3A). Equation 1 was used again to fit the obtained fluorescence data (Figure 3B). The "in vivo calibration" procedure, essential for estimation of the intracellular IP_3 concentration ($[IP_3]_i$) from the obtained emission data, revealed that the *Kd* value is 1.24 μM in Equation 1 and that the in vivo dynamic range of the probe is approximately 0.5–5 μM $[IP_3]_i$. It is also important to note that the data clearly demonstrate rapid and efficient response of the sensor to increase of $[IP_3]_i$ in vivo.

In B lymphocytes, ligation of B cell receptors (BCR) with anti-IgM antibody (anti-IgM) evokes activation of PLCγ_2, IP_3 production, and Ca^{2+} release and entry [33]. Without BCR ligation, intensity of fluorescence at an emission wavelength of 510 nm gradually decreased

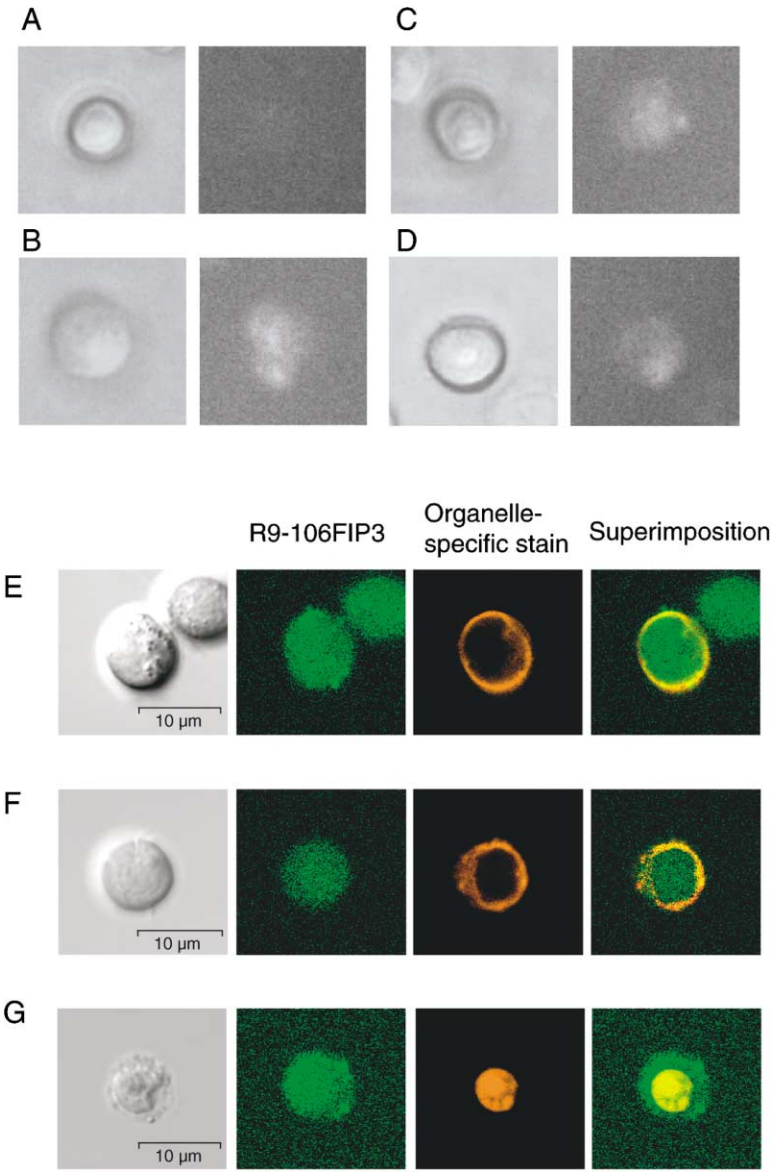

Figure 2. Intracellular Distribution of the IP_3 Sensor R9-106DIP3

(A–D) Incorporation of the Tat-related peptide-fused sensors into DT40 cells. Cells were incubated with untagged IP_3 sensor (106DIP3) (A), Tat-106DIP3 (B), R7-106DIP3 (C), and R9-106DIP3 (D). Left, DIC images of DT40 cells; right, fluorescent images of the same cells.

(E–G) Cellular localization of R9-106FIP3 in DT40 cells. Confocal microscopic observation of the R9-106FIP3-loaded cells after organelle-specific staining. The fluorescein version of the sensor R9-106FIP3 [16] was used because organelle-specific probes and R9-106DIP3 have similar excitation wavelengths. (E), membrane staining with octadecyl rhodamin B; (F), ER staining with DiI16; (G), nucleus staining with propidium iodide (PI). For PI staining, cells were permeabilized with β-escin after incorporation of R9-106FIP3.

in wild-type (WT) and PLCγ_2-deficient (PLCγ_2^-) chicken DT40 B-cells loaded with R9-106DIP3 (Figure 3C). This seems to reflect degradation of the photo-labile R9-106DIP3 by UV irradiation during the measurement, since increase of interval of UV irradiation reduced the reduction speed of fluorescence intensity. Speeds of fluorescence reduction elicited by UV irradiation at 2, 10, and 20 s intervals were 135%, 77%, and 63%, respectively, of the speed at the 5 s interval routinely used in the measurement. Within 20 s after BCR ligation, significant speeding up of florescence decrease, namely IP_3 production ($\Delta[IP_3]_I$, Figures 3C and 3D) and $[Ca^{2+}]_i$ rises mediated by IP_3R release channel [33] in WT cells, were observed coincidentally (Figure 3E). In contrast, PLCγ_2^- cells never showed these responses. Interestingly, fluorescence intensity changes in R9-106DIP3-loaded DT40 cells were significantly affected by extracellular Ca^{2+}: decrease in fluorescence intensity was maintained after an initial decrease indicative of sustained $[IP_3]_i$ increase in Ca^{2+}-containing external solution, whereas fluorescence intensity decreased only transiently to return to almost initial levels in Ca^{2+}-free external solution (Figure 3D). The observed changes in fluorescence intensity of R9-106DIP3 showed an interesting temporal correlation with the BCR-induced $[Ca^{2+}]_i$ transients (Figures 3D and 3E). R9-106DIP3 fluorescence recovery ($[IP_3]_i$ decrease) delayed compared to decay of $[Ca^{2+}]_i$ transients. The results strongly support detection of IP_3 increase and decrease by sensor R9-106DIP3 through reversible IP_3 binding, suggesting that IP_3 production is positively regulated by Ca^{2+} entry.

Efficiency of R9-106DIP3 was also examined in other cell types. As shown in Figure 4A, stimulation of G protein-coupled ATP receptors induced transient $[IP_3]_i$ increases in the absence of extracellular Ca^{2+} in CHO cells loaded with R9-106DIP3. Subsequent addition of Ca^{2+} to external solution induced additional $[IP_3]_i$ increases. This observation is quite similar to that observed in DT40

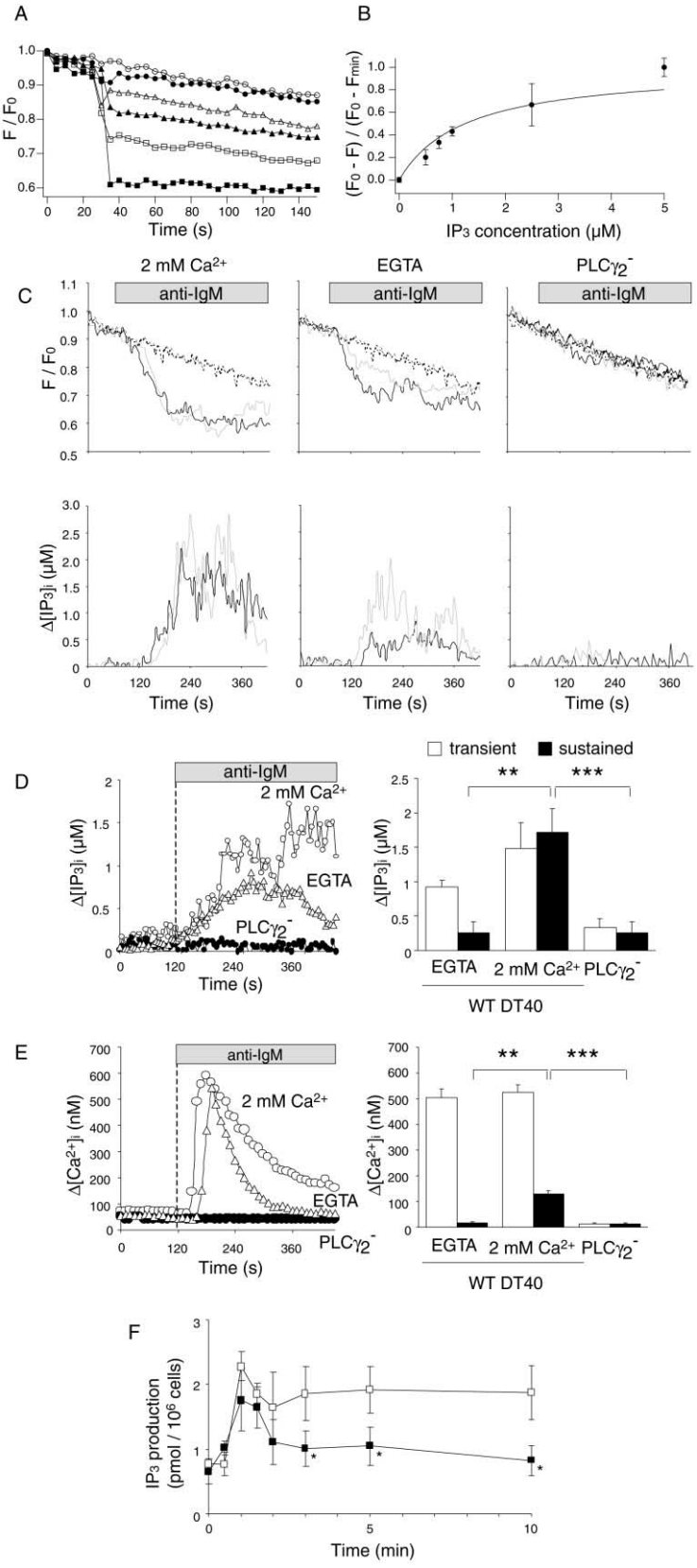

Figure 3. In Vivo IP_3 Detection by R9-106DIP3

(A) Time courses of fluorescence changes of R9-106DIP3 by adding 0 (open circles), 0.5 (filled circles), 0.75 (open triangles), 1 (filled triangles), 2.5 (open squares), and 5 μM (filled squares) IP_3 in the DT40 cell permeabilized with β-escin.

(B) The changes in the fluorescence intensity were plotted against IP_3 concentrations. A solid curve represents the best fit for Equation 1.

(C) Real-time measurements of intracellular receptor-mediated IP_3 production ($\Delta[IP_3]_i$) in DT40 cells. The upper panels show representative time courses of fluorescence intensity changes of IP_3 indicator monitored at 5 s intervals upon B cell receptor (BCR) stimulation. Bars show times of BCR stimulation with anti-IgM antibody (anti-IgM: 1 μg/ml). The dotted traces indicate the time course of photo-bleaching of IP_3 sensor. Other traces represent time courses of fluorescence changes observed in individual BCR-stimulated cells. The lower panels show time courses of IP_3 concentration changes. The changes of the fluorescence intensities in the upper panels were normalized with the time courses of photo-bleaching of the IP_3 sensor and were converted to the changes of IP_3 concentration by using the in vivo calibration curve in (B).

(D) Left, average time courses of IP_3 concentration changes induced by BCR stimulation in WT (open circles) and PLCγ2-deficient PLCγ2$^-$ DT40 cells (filled circles) in the presence or absence (open triangles) of extracellular Ca^{2+}. Treatment with anti-IgM started at the time indicated by the dotted line. For the experiments in the absence of Ca^{2+}, perfusion of EGTA-containing solution was started 2.5 min before BCR stimulation and was continued to the end of experiment. Right, $\Delta[IP_3]_i$ by BCR stimulation at the peak point (transient) and sustained after 6 min BCR stimulation (sustained). Data points are the mean ±SE in 17–22 cells. Significance from control (2 mM Ca^{2+}): **, $p < 0.01$; ***, $p < 0.001$.

(E) Left, time courses of Ca^{2+} responses upon BCR stimulation in WT (open circles) and PLCγ2-deficient PLCγ2$^-$ DT40 cells (filled circles) in the presence or absence (open triangles) of extracellular Ca^{2+}. Protocols used were the same as in (D). Right, peak $[Ca^{2+}]i$ rises by BCR stimulation. Data points are the mean ±SE in 35–62 cells ($[Ca^{2+}]_i$).

(F) Population measurements of BCR-induced IP_3 production in DT40 cells in the presence (open squares) or absence (closed squares) of extracellular Ca^{2+}. Significance from control (2 mM Ca^{2+}): *, $p < 0.05$.

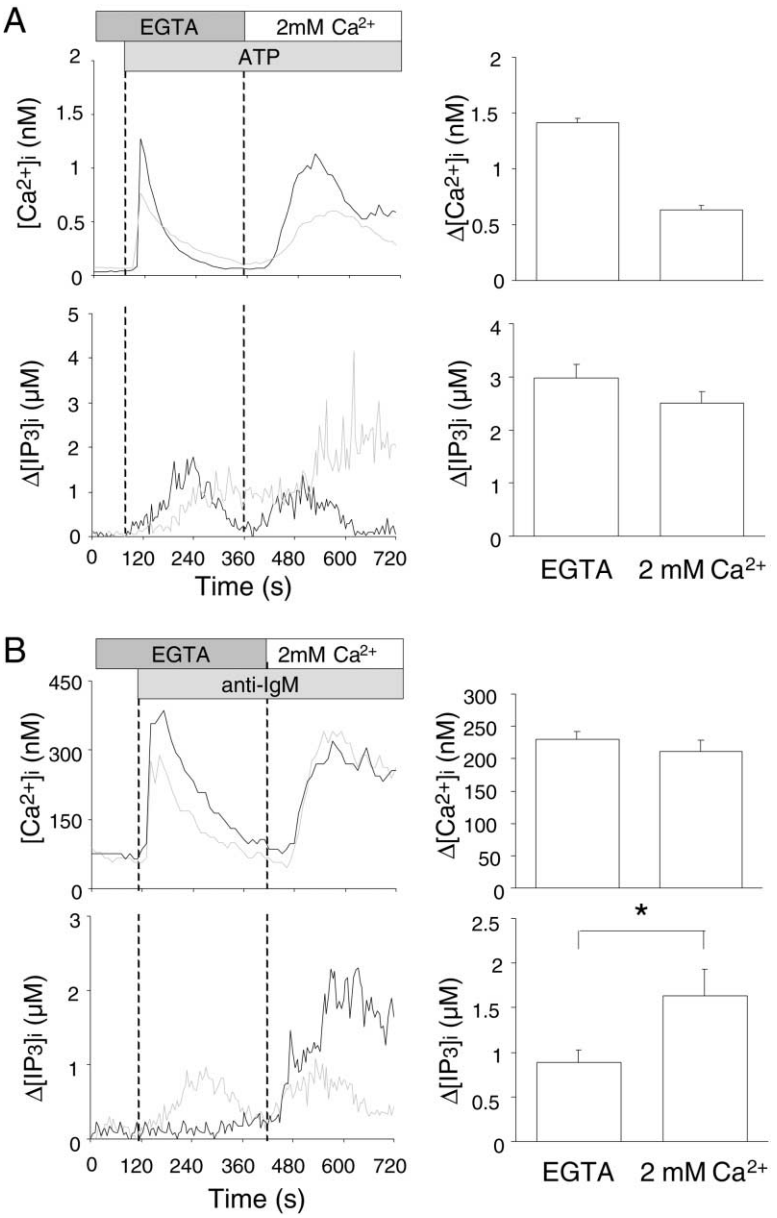

Figure 4. Major Contribution of Ca^{2+} Influx to Receptor-Evoked IP_3 Production

(A) Left, representative time courses of Ca^{2+} responses (upper) and IP_3 production (lower) induced by stimulation of Gq-coupled ATP receptor with ATP (10 μM) in Ca^{2+}-free solution containing EGTA and by subsequent addition of 2 mM extracellular Ca^{2+} to evoke capacitative Ca^{2+} entry in CHO-K1 cells. Traces represent time courses of $[Ca^{2+}]_i$ and $[IP_3]_i$ changes observed in individual receptor-stimulated cells. Bars indicate times of perfusion with respective solutions, and Ca^{2+}-free solution was perfused 2.5 min before the ATP treatment. Right, peak $[Ca^{2+}]_i$ and $[IP_3]_i$ rises by ATP receptor stimulation. Data points are the mean ±SE in 24 cells ($[Ca^{2+}]_i$) or in 14 cells ($[IP_3]_i$).

(B) Left, representative time courses of Ca^{2+} responses (upper) and IP_3 production (lower) induced by BCR stimulation in the presence or absence of extracellular Ca^{2+}. The BCR stimulation starts at the time indicated by the dotted line, and Ca^{2+}-free EGTA-containing solution was perfused from 2.5 min before BCR stimulation. Right, peak $[Ca^{2+}]_i$ and $[IP_3]_i$ rises by the BCR stimulation. Data points are the mean ±SE in 31 cells ($[Ca^{2+}]_i$) or the mean ± SE in 17 cells ($[IP_3]_i$). *, $p < 0.05$.

cells (Figure 4B). Considering that the protocol used to assess the real-time effect of Ca^{2+} entry on IP_3 generation is only realized in the intact cellular configuration, R9-106DIP3 can serve as an efficient sensor for direct detection of in vivo regulation of IP_3 production.

We next tested whether loaded R9-106DIP3 perturbs Ca^{2+} responses upon BCR stimulation in DT40 B cells. The cells loaded with the sensor analog R9-106FIP3 conjugated with fluorescein [16] were also tested, since R9-106FIP3-unloaded cells can be distinguished from the loaded cells in $[Ca^{2+}]_i$ measurements owing to the difference in excitation wavelength between R9-106FIP3 and the Ca^{2+} indicator fura-2. The data indicate that cells incubated with R9-106DIP3 or loaded with R9-106FIP3 showed BCR-induced Ca^{2+} responses indistinguishable from those in control cells (Figure 5A). By contrast, DT40 cells expressing the genetically encoded GFP-based phosphoinositide probe, PLCδ PH domain-GFP fusion protein (PH-GFP) [13–15], showed significantly suppressed BCR-induced Ca^{2+} responses. Thus, loaded R9-106DIP3 may have significantly low IP_3-buffering capacity, which enables accurate measurement of $[IP_3]_i$ changes without significantly affecting receptor-activated cellular responses.

Discussion

We have developed biosensors for direct and real-time detection of $[IP_3]_i$ changes by combining recombinant DNA technique and chemical modification with fluorophores. The newly developed IP_3 probe R9-106DIP3 showed improved cellular incorporation and efficient detection of IP_3 in various types of cells. The probe has merit compared to recently described GFP fusion

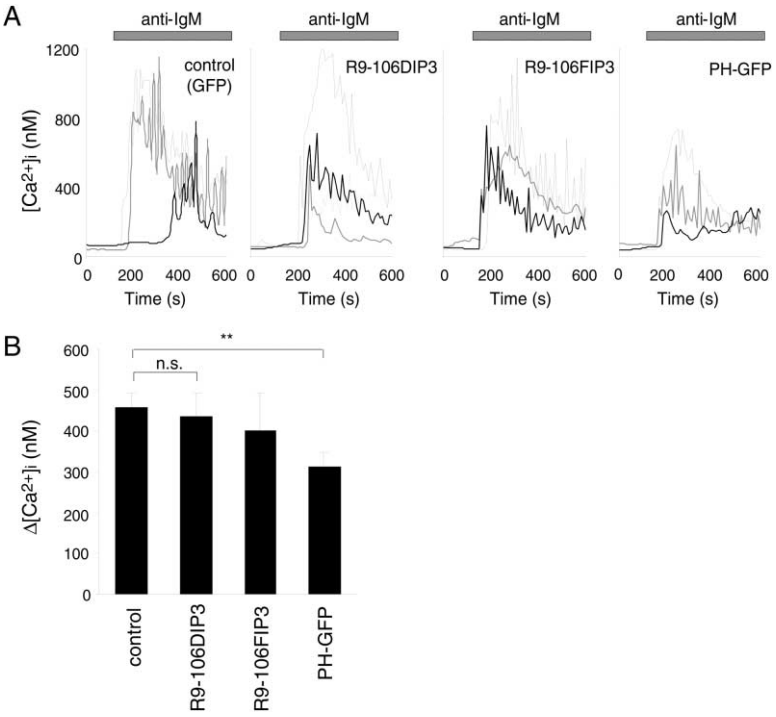

Figure 5. The Original PH Domain Perturbs but the IP_3 Sensors Keep Receptor-Evoked $[Ca^{2+}]_i$ Responses Intact

(A) Representative time courses of $[Ca^{2+}]_i$ responses induced by BCR stimulation in individual control GFP-expressing or PH-GFP-expressing DT40 cells and R9-106DIP3 or R9-106F-loaded cells.

(B) Summary of peak $[Ca^{2+}]_i$ rises induced by BCR stimulation in cells expressing the constructs or loaded with the sensors above. Data are the mean ± SE in 22–46 cells. n.s., not significant; significance from control (GFP): **, $p < 0.01$.

protein probes [13]. R9-106DIP3 is selective for IP_3 over other inositol phosphates and the phosphoinositide, which allows us to quantitatively transform IP_3 binding-induced fluorescence quenching of R9-106DIP3 into IP_3 concentration through an in vivo calibration procedure. In contrast to R9-106PIP3, the GFP-tagged PH domain probe similarly detects IP_3 and PIP_2. The observed receptor stimulation-induced translocation of the GFP-tagged PH probe from plasma membrane to cytoplasm has been therefore interpreted to represent PIP_2 metabolism at the plasma membrane and subsequent $[IP_3]_i$ diffusion throughout the cytoplasm [14]. Furthermore, it has been pointed out that stable overexpression of the genetically encoded probes can significantly change the molecular geography by sequestration of inositol lipids and might exert inhibitory effects on various lipid-dependent cellular functions [13]. In R9-106DIP3, this type of problem can be avoided by controlling the amount of the probe loaded. The lower binding affinity of R9-106DIP3 with inositol phosphates other than IP_3 and phosphoinositides in comparison to the original PH domain from PLCδ also minimizes side effects during measurement (Figure 5). This advantage of R9-106DIP3 is attributable to the fluorophore conjugation of the cysteine residue at the mouth of the IP_3 binding pocket [16]. In fact, the data indicate that cells loaded with the IP_3 sensor were indistinguishable from control cells in BCR-induced Ca^{2+} responses measured using the fura-2 method (Figures 5A and 5B), whereas the cells expressing the genetically encoded GFP-based phosphoinositide probe PH-GFP [13–15] showed significantly suppressed BCR-induced Ca^{2+} responses (Figures 5A and 5B). Thus, R9-106DIP3 is the first IP_3 sensor that simultaneously realized selectivity and directness of IP_3 detection and intactness of the cells examined.

R9-106DIP3 and the previously reported "single cell" probes [13, 14] display an interesting contrast in cellular compartmentalization. Rapid loss within 30 s of PH-GFP probes from the plasma membrane is induced by ATP receptor stimulation [13, 14], suggesting high sensitivity of PH-GFP in PIP_2 hydrolisis/IP_3 production at the plasma membrane. R9-106DIP3 incorporated diffusively in cells (Figure 2) revealed probe fluorescence decrease/IP_3 production without specific compartmentalization when the probe fluorescence was monitored at a 5 s interval. This is consistent with our observation that IP_3 concentrations are equilibrated within 5 s after extracellular IP_3 application in permeabilized cells (Figure 3A), as well as with the report by Allbritton et al. [34] that IP_3 is a global messenger distributed in cells smaller than 20 μm, in contrast to Ca^{2+} acting in restricted subcellular domains. Thus, R9-106DIP3 and other "single cell" probes, including the α-hemolysin-based IP_3 detection method that senses nanomolar IP_3 localized near the plasmamembrane [35], will provide complementary information with regard to spatial/temporal patterns of IP_3 signals.

R9-106DIP3 has an advantage with regard to significantly low buffering of IP_3 signals by the probe itself. This is supported by the fact that lowering the probe concentration from 1 to 0.25 μM failed to significantly affect receptor-induced IP_3 responses (Figure S2B). In the formation of the 1:1 complex of IP_3 and the probe, 1.21 μM is obtained for *Kd* by fitting *F/F0* from the Figure 2A data to Equation 2:

$$F/F_0 = 1 - A \times \{Kd + [IP_3]_t + C - ([IP_3]_t^2 + 2[IP_3]_t Kd - 2C[IP_3]_t + 2CKd + C^2 + Kd^2)^{1/2}\}/(2C), \quad (2)$$

in which $[IP_3]_t$, *A*, and *C* are total intracellular IP_3 concentration, the maximal changes in normalized fluorescence intensity $[(F_{max} - F_{min})/F_{max}]$, and the concentration of the incorporated probe, respectively [36]. When $[IP_3]_t$ is 3 μM, the above *Kd* value gives 71 nM for the IP_3-R9-106DIP3 complex concentration ([complex]) using $Kd = [IP_3][R9\text{-}106DIP3]/[complex]$, since we estimated *C* to be 100 nM in the cells loaded with the probe in 1 μM solution through comparison of their fluorescence intensities with those of the probe at various concentrations in between pairs of glass cover slips (data not shown). Therefore, only less than 1/40 of IP_3 produced is buffered by the probe itself, again supporting the efficiency of R9-106DIP3 in being significantly free from interfering native IP_3 signaling.

R9-106DIP3 has enabled the first real-time demonstration of positive regulation of IP_3 production by receptor-activated Ca^{2+} influx in individual cells. A previous report determining IP_3 levels by competition assay with $[^3H]IP_3$ using destroyed cells has demonstrated enhancement of IP_3 production by Ca^{2+} entry via $PLC\delta_1$ [37]. However, it was difficult to temporally correlate IP_3 production with $[Ca^{2+}]_i$, since the highest time resolution was 15 s in the experiment. In addition, the data were averaged behavior of different masses of cells but were not from the same individual cells. In contrast to the population measurement, our data using R9-106DIP3 clearly demonstrate delay of $[IP_3]_i$ decrease compared to decay of $[Ca^{2+}]_i$ transients in individual cells, suggesting that a negative regulation signal for Ca^{2+} response is generated during PIP_2 hydrolysis. Interestingly, the $[IP_3]_i$ measurement using R9-106DIP3 demonstrated a gradual increase of $[IP_3]_i$ in Ca^{2+}-containing external solution and a slow $[IP_3]_i$ increase, peaking only after 2 min BCR stimulation in Ca^{2+} free-external solution (Figure 3D), while BCR-induced IP_3 production in the IP_3 population measurement using lysed cells showed a peak after 1 min stimulation in DT40 cells (Figure 3F). Considering rapid association/dissociation kinetics of IP_3 with the probe in in vitro experiments, it is possible that this discrepancy between the two methods is attributable to the difference in IP_3 fraction detected by the methods: R9-106DIP3 detects free IP_3, but the population measurement detects free IP_3 plus IP_3 buffered by IP_3 binding proteins. Given that the diameter of DT40 cells is ~10 μm, estimation from the population measurement actually gives $\Delta[IP_3]_i$ of ~2.7 μM (~1.5 and ~4.2 μM for basal and peak $[IP_3]_I$, respectively), which is slightly higher than that obtained from the single cell measurement. In this context, IP_3-buffering mechanisms can be downregulated after 1 min B cell receptor stimulation, since free $[IP_3]_i$ was kept elevated (Figure 3D), while the total $[IP_3]_i$ (free $[IP_3]_i$ plus buffered $[IP_3]_i$) was decreased (Figure 3F). Alternatively, the above discrepancy may be due to differences in the stimulation condition: cells were perfused with anti-IgM-containing PSS at room temperature in the single cell measurements, while anti-IgM was added and immediately mixed with cell suspension of PSS at 37°C in the population measurement (see Experimental Procedures).

It must be further noted that our data show recovering of fluorescence intensity of R9-106DIP3 after initial decrease in response to receptor stimulation in the tested cell types such as DT40, HEK, and CHO cells. This supports sufficient reversibility in binding of IP_3 with the probe, which may reflect $[IP_3]_i$ oscillation [14]. Thus, R9-106DIP3 is efficient in quantitative and temporal assessment of $[IP_3]_i$ changes. Although the $[IP_3]_i$ measurement is still open to further refinement by employing more sophisticated techniques, such as caged IP_3 derivatives [38] for calibration, R9-106DIP3 is no doubt already a powerful tool for understanding the complex interplay among different second messengers in various biological systems.

Significance

The second messenger D-myo-inositol-1,4,5-trisphosphate (IP_3) regulates intracellular Ca^{2+} concentration. Mapping real-time intracellular IP_3 concentration changes is an indispensable technique to elucidate the diverse cellular processes related to IP_3 production. We have developed a biosensor for direct and real-time detection of intracellular IP_3 concentration changes based on binding by the PLCδ PH domain. The IP_3 sensor tagged with the arginine-rich peptide was efficiently incorporated into intact cells and detected the intracellular IP_3 concentration changes induced by ATP stimulation of CHO cells or anti-IgM antibody stimulation of DT40 cells. The IP_3 biosensor reported here would be a powerful tool for detecting positive regulation of IP_3 production by receptor-activated Ca^{2+} influx, which can be only elicited in the intact cellular configuration. The concept of the biosensor design, based on fluorophore conjugation at the mouth of binding pockets of small protein domains, is applicable for other second messengers, providing important tools for elucidating metabolism networks of second messengers.

Experimental Procedures

Plasmid Constructs

cDNA encoding the PH domain of $PLC\delta_1$ (11-140) was amplified with PCR from rat brain cDNA library (CLONTECH Labs. Inc.) and subcloned into pET3a vector to yield pET3PH as described previously [16]. The mutated PH domain (Cys48, Cys96, and Asn106 to Ser48, Ser98, and Cys106, respectively) was created by using PCR-based site-directed mutagenesis, and expression constructs of TAT (YGRKKRRQRRR), arginine nonapeptide (R_9), and arginine heptapeptide (R_7) fused with the mutated PH domain were generated by inserting double-strand oligonucleotides encoding the amino acid sequences of TAT, R_9 and R_7 peptides, respectively, into pET3PH106 vector [16].

Protein Purification and Fluorophore Coupling Reactions

The plasmids were transformed into *Escherichia coli* BL21(DE3)-pLysS cells, and the proteins were purified by using Mono S cation exchange chromatography (Amersham Pharmacia) with 10 mM phosphate buffer (pH 7.0) containing 50 mM NaCl and 4 M urea. Fractions containing mutated PH domain were collected. The solution (1 ml) containing the mutated PH domain (10 μM) was degassed and was added to a DMF solution of 6-bromoacetyl-2-dimethylaminonaphthalene (DAN) or 6-iodoacetamidofluorescein (6IAF) known as thiol reactive fluorophore (10 eq.) at 4°C. After 2.5 hr, the reaction was quenched by addition of DTT to a final concentration of 5 mM. The labeled protein was separated from free fluorophore by gel filtration using a PD-10 column with 10% acetonitrile containing 0.1% TFA, purified by using RESOURCE RPC reversed phase chromatography, then dialyzed against a phosphate buffer (pH 7.0) con-

taining 50 mM NaCl and 0.005% Tween 20. The purified fluorophore-labeled PH domains were identified by 15% SDS/polyacrylamide gel visualized with transilluminator or with Coomassie Brilliant Blue R-250 (CBB) staining.

PIP_2 Binding Assay

PIP_2 resin (Echelon) was incubated with 0.5 μM R9-106DIP3 (R_9-tagged PH domain conjugated with DAN fluorophore at the cysteine residue 106) and the PH domain of PLCδ$_1$ (PLCδ$_1$ PH)(11-140) for 5 min at room temperature in 10 mM phosphate (pH 8.0) containing 100 mM NaCl and 0.01% Tween 20. After the PIP_2 resin was separated from the supernatant (**S**, nonbinding fraction) by centrifugation at 1000 × g for 1 min at room temperature, R9-106DIP3 or PLCδ$_1$ PH was eluted from the PIP_2 resin with 10 mM phosphate (pH 8.0), 100 mM NaCl, and 0.01% Tween 20 containing 50 μM IP_3 to give binding fraction (**B**). The nonbinding fraction (**S**) and **B** were precipitated by adding an equal volume of 20% trichloroacetic acid and centrifugation and were quantitated by analyzing 15% SDS-polyacrylamide gel electrophoresis followed by CBB staining. In detail, the quantification of each band was performed by analyzing the scaled gel data with NIH Image (ver. 1.6) software to integrate the intensity of dots of which each band was composed. The binding fractions Q = [**B**]/([**B**] + [**S**]) for R9-106DIP3 and PLCδ$_1$ PH to the PIP_2 resin were plotted against the PIP_2 concentrations. A solid curve represents the best fit for a theoretical dissociation equation, $Q_{fit} = [PIP_2]_{total}/(Kd + [PIP_2]_{total})$, where $[PIP_2]_{total}$ is the total concentration of PIP_2 and *Kd* is the dissociation constant of the protein-PIP_2 complex.

In Vitro Fluorescent Measurements

Binding reactions of R9-106DIP3 and IP_3 were monitored by measuring the changes in fluorescence emission that occurred upon addition of IP_3 to a solution of 100 nM R9-106DIP3 in 10 mM phosphate buffer (pH 7.0) containing 50 mM NaCl and 0.005% Tween 20 at 25°C. Fluorescence emission spectra were recorded by addition of increasing amounts of IP_3 to saturation at the excitation wavelength at 390 nm. The dissociation constant of the complex of R9-106DIP3 and IP_3 was determined by measuring the change in fluorescence emission at a wavelength of 500 nm. The results were fit to a binding isotherm,

$$\Delta F = \Delta F_{max} \{[IP_3]/(Kd + [IP_3])\}, \quad (1)$$

where ΔF is the change in fluorescence intensity, ΔF_{max} is the fluorescence intensity change at saturation, *Kd* is the dissociation constant, and $[IP_3]$ is the concentration of IP_3.

Kinetic Determination of Dissociation Constants for the 106DIP3 Complex by Surface Plasmon Resonance

A biotin-labeled IP_3 was injected over a streptavidin-coated sensor chip (SA, Pharmacia Biosensor) until a suitable level was achieved. A buffer containing 10 mM HEPES, 150 mM NaCl, 3.4 mM EDTA, and 0.005% Tween 20 was used both as flow buffer and sample preparation buffer. The same buffer containing 1 mM IP_3 was used as regeneration buffer. The association was followed for 3 min, and the dissociation was measured at a flow rate of 20 μl/min. Analysis of the data was performed using the evaluation software supplied with the instrument (BIAevaluation version 3.0). To eliminate small bulk refractive change differences at the beginning and end of each injection, a control sensorgram obtained over a surface modified with biotin was subtracted for each peptide injection. Furthermore, the second phase of the responses were fitted, since instrument response contains a component due to the change in bulk refractive index of the two solutions (i.e., soluble ligate versus buffer) during the first 20–30 s period after injection of ligate, as described by O'Shannessy et al. [39]. For the determination of the dissociation kinetics constant (*k*d),

$$RU(t) = RU_0 \cdot e^{(-kd \cdot t)} \quad (3)$$

was used. RU(t) and RU_0 are the response at the optional time and the response at the time at which dissociation begins, respectively.

IP_3 Sensor Incorporation

For each assay, 5 × 10^4/ml DT40 cells were pelleted on a 10 mm × 5 mm glasses and cultured for 3–4 hr. Chinese hamster ovary (CHO)-K1 cells were trypsinized, diluted with F-12 medium containing 10% fetal bovine serum (FBS), 30 units/ml penicillin, and 30 μg/ml streptomycin and plated onto glass coverslips precoated with poly-L-lysine (Sigma) at least 6 hr. After complete adhesion, the solution containing IP_3 sensor was exchanged for Hanks' balanced salt solution (HBSS, Sigma) containing 0.1% F127 (Molecular Probes) using a NAP5 column (Amersham Pharmacia). The cells were incubated into 1 μM IP_3 sensor solution for 10 min at room temperature (Figure S2A). Cells were washed with HBSS, and the distribution of IP_3 sensor was observed at an emission wavelength of 500 nm at room temperature by exciting at 385 nm on a fluorescence microscope (Olympus, Japan).

Subcellular Localization of IP_3 Sensor Probe

DT40 cells (5 × 10^4) were plated and cultured for 4 hr on 30 mm plates on a glass coverslip. The culture medium was discarded, and the cells were washed with HBSS (Sigma). HBSS buffer was discarded, and the cells were incubated with the HBSS buffer containing 1 μM R9-106FIP3 (R_9-tagged PH domain conjugated with fluorescein at the cysteine residue 106) and 0.1% F127 (Molecular Probes) for 10 min at 37°C. After the cells were washed with HBSS buffer, the cells were incubated with HBSS buffer containing 0.1 μM octadecyl rhodamin B or 0.1 μM DiI16 (Molecular Probes) for 2 min at 37°C. For the staining of nucleus, 0.1 μM propidium iodide (PI) (Dojindo) was incubated with cells for 2 min after 10 min treatment of R9-106FIP3-preloaded cells with β-escin (1 μM, Sigma). After the cells were washed with HBSS buffer, the distribution of fluorescenes was analyzed under a confocal laser microscope (FV500, Olympus). Excitation wavelength: 488 nm for fluorescein and 543 nm for octadecyl rhodamin B, DiI16, and PI. Emission wavelength: 518 nm for fluorescein and 578, 565, and 617 nm for octadecyl rhodamin B, DiI16, and PI, respectively.

In Vivo Fluorescent Measurements

The cells (5 × 10^4 cells/ml) were plated onto poly-L-lysine-coated glass coverslips. After 2 hr incubation for cell adhesion, the cells were transferred to HBSS containing 1 μM IP_3 sensor and 0.1% F127 (Molecular Probes) for 10 min at 37°C. After cells were washed with HBSS, the coverslips were placed in a perfusion chamber mounted on the stage of the microscope. Cells in the chamber with a capacity of 500 μl were perfused with various solutions with a rate of 500 μl/min. Changes in fluorescence images of the cells were observed using a video image analysis system at an emission wavelength of 510 nm (bandwidth, 20 nm) at room temperature by exciting at 380 nm (bandwidth, 11 nm) in a physiological salt solution (PSS) containing (in mM) 150 NaCl, 4 KCl, 1 $MgCl_2$, 2 $CaCl_2$, 5.6 glucose, 5 HEPES adjusted to pH 7.4 with NaOH. $[IP_3]_i$ increases were detected as fluorescence quenching of R9-106DIP3 due to IP_3 binding. All traces except those of Figures 3A and 3C were displayed after subtracting averaged time courses of fluorescence reduction obtained without cell stimulation attributable to photo-bleach or photo-degradation.

For the in vivo calibration of $[IP_3]_i$, synthesized IP_3 (Dojindo) was applied to DT40 cells after 10 min treatment of R9-106DIP3-preloaded cells with β-escin (1 μM, Sigma). The initial decrease of fluorescence was observed, and the results were fit to Equation 1. The $[IP_3]_i$ was calculated on the basis of Equation 1, where *Kd* value is 1.24 μM obtained by in vivo calibration experiment.

Measurement of Changes in Intracellular Free Ca^{2+} ($[Ca^{2+}]_i$)

CHO-K1 cells on coverslips were loaded with fura-2 by incubation in F-12 containing 5 μM fura-2/AM, 0.2% F127 and 10% FBS at 37°C for 30 min and washed with the HEPES-buffered saline (HBS) containing (in mM): 107 NaCl, 6 KCl, 1.2 $MgSO_4$, 2 $CaCl_2$, 1.2 KH_2PO_4, 11.5 glucose, and 20 HEPES adjusted to pH 7.4 with NaOH. DT40 cells were prepared according to the previous paper [40]. The coverslips were then placed in a perfusion chamber mounted on the stage of the microscope, and cells were perfused with solutions as described above in IP_3 measurements. Fluorescence images of the cells were recorded and analyzed with a video image analysis sys-

tem (ARGUS-20/CA, Hamamatsu Photonics, Hamamatsu, Japan). The fura-2 fluorescence at an emission wavelength of 510 nm (bandwidth, 20 nm) was observed at room temperature by exciting fura-2 alternatingly at 340 and 380 nm (bandwidth, 11 nm). The 340/380 nm ratio images were obtained on a pixel by pixel basis and were converted to Ca^{2+} concentrations by in vivo calibration. The calibration procedure was performed according to previous reports [40, 41].

Population Measurement for IP_3 Production

Population IP_3 production assay was performed as described previously [37]. DT40 cells (1×10^6) were suspended in 50 μl serum-free PSS solution, and anti-IgM (2 μg) was added to the cell suspension and incubated for the indicated time at 37°C. The BCR stimulation was terminated by adding 50 μl trichloroacetic acid (15%). After extraction with diethyl ether and subsequent pH adjustment to 7.5 with 0.5 M $NaHCO_3$, samples were subjected to kinetic analysis of IP_3 production using the BIOTRAK IP_3 assay system. Assay was performed according to the manufacturer's instructions (Amersham Pharmacia Biotech).

Statistical Analysis

Results are presented as means ± S.E.M. obtained through observations of n cells in at least three independent experiments. The statistical significance of observed differences was determined by analysis of variance followed by Student's t test. Differences among means were considered significant when p was less than 0.05.

Supplemental Data

Two figures are available as supplemental data at http://www.chembiol.com/cgi/content/full/11/4/475/DC1.

Acknowledgments

We thank Keiji Imoto for helpful discussion.

Received: October 27, 2003
Revised: January 2, 2004
Accepted: January 9, 2004
Published: April 16, 2004

References

1. Tsien, R.W., and Tsien, R.Y. (1990). Calcium channels, stores, and oscillations. Annu. Rev. Cell Biol. *6*, 715–760.
2. Clapham, D.E. (1995). Calcium signaling. Cell *80*, 259–268.
3. Berridge, M.J. (1993). Inositol trisphosphate and calcium signalling. Nature *361*, 315–325.
4. Bootman, M.D., and Berridge, M.J. (1995). The elemental principles of calcium signaling. Cell *83*, 675–678.
5. Neher, E. (1992). Cell physiology. Controls on calcium influx. Nature *355*, 298–299.
6. Fasolato, C., Innocenti, B., and Pozzan, T. (1994). Receptor-activated Ca^{2+} influx: how many mechanisms for how many channels? Trends Pharmacol. Sci. *15*, 77–83.
7. Putney, J.W., Jr. (1990). Capacitative calcium entry revisited. Cell Calcium *11*, 611–624.
8. Irvine, R.F. (1990). 'Quantal' Ca^{2+} release and the control of Ca^{2+} entry by inositol phosphates: a possible mechanism. FEBS Lett. *263*, 5–9.
9. Peppelenbosch, M.P., Tertoolen, L.G., den Hertog, J., and de Laat, S.W. (1992). Epidermal growth factor activates calcium channels by phospholipase A2/5-lipoxygenase-mediated leukotriene C4 production. Cell *69*, 295–303.
10. Binder, H., Weber, P.C., and Siess, W. (1985). Separation of inositol phosphates and glycerophosphoinositol phosphates by high-performance liquid chromatography. Anal. Biochem. *148*, 220–227.
11. Potter, B.V.L., and Lampe, D. (1995). Chemistry of inositol lipid mediated cellular signaling. Angew. Chem. Int. Ed. Engl. *34*, 1933–1972.
12. Palmer, S., Hughes, K.T., Lee, D.Y., and Wakelam, M.J. (1989). Development of a novel, Ins(1,4,5)P_3-specific binding assay. Its use to determine the intracellular concentration of Ins(1,4,5)P_3 in unstimulated and vasopressin-stimulated rat hepatocytes. Cell. Signal. *1*, 147–156.
13. Balla, T., Bondeva, T., and Varnai, P. (2000). How accurately can we image inositol lipids in living cells? Trends Pharmacol. Sci. *21*, 238–241.
14. Hirose, K., Kadowaki, S., Tanabe, M., Takeshima, H., and Iino, M. (1999). Spatiotemporal dynamics of inositol 1,4,5-trisphosphate that underlies complex Ca^{2+} mobilization patterns. Science *284*, 1527–1530.
15. Stricker, R., Adelt, S., Vogel, G., and Reiser, G. (1999). Translocation between membranes and cytosol of p42IP_4, a specific inositol 1,3,4,5-tetrakisphosphate/phosphatidylinositol 3,4, 5-trisphosphate-receptor protein from brain, is induced by inositol 1,3,4,5-tetrakisphosphate and regulated by a membrane-associated 5-phosphatase. Eur. J. Biochem. *265*, 815–824.
16. Morii, T., Sugimoto, K., Makino, K., Otsuka, M., Imoto, K., and Mori, Y. (2002). A new fluorescent biosensor for inositol trisphosphate. J. Am. Chem. Soc. *124*, 1138–1139.
17. Anderson, D.C., Nichols, E., Manger, R., Woodle, D., Barry, M., and Fritzberg, A.R. (1993). Tumor cell retention of antibody fab fragments is enhanced by an attached HIV TAT protein-derived peptide. Biochem. Biophys. Res. Commun. *194*, 876–884.
18. Fawell, S., Seery, J., Daikh, T., Moore, C., Chen, L.L., Pepinsky, B., and Barsoum, J. (1994). Tat-mediated delivery of heterologous proteins into cells. Proc. Natl. Acad. Sci. USA *91*, 664–668.
19. Pepinsky, R.B., Androphy, E.J., Corina, K., Brown, R., and Barsoum, J. (1994). Specific inhibition of a human papillomavirus E2 trans-activator by intracellular delivery of its repressor. DNA Cell Biol. *13*, 1011–1019.
20. Kim, D.T., Mitchell, D.J., Brockstedt, D.G., Fong, L., Nolan, G.P., Fathman, C.G., Engelman, E.G., and Rothbard, J.B. (1997). Introduction of soluble proteins into the MHC class I pathway by conjugation to an HIV tat peptide. J. Immunol. *159*, 1666–1668.
21. Vives, E., Brodin, P., and Lebleu, B. (1997). A truncated HIV-1 tat protein basic domain rapidly translocates through the plasma membrane and accumulates in the cell nucleus. J. Biol. Chem. *272*, 16010–16017.
22. Vives, E., Granier, C., Prevot, P., and Leblue, B. (1997). Structure and activity relationship study of the plasma membrane translocating potential of a short peptide from HIV-1 Tat protein. Lett. Pept. Sci. *4*, 429–436.
23. Derossi, D., Chassaing, G., and Prochiantz, A. (1998). Trojan peptides: the penetratin system for intracellular delivery. Trends Cell Biol. *8*, 84–87.
24. Nagahara, H., Vocero-Akbani, A.M., Snyder, E.L., Ho, A., Latham, D.G., Lissy, N.A., Becker-Hapak, M., Ezhevsky, S.A., and Dowdy, S.F. (1998). Transduction of full-length TAT fusion proteins into mammalian cells: TAT-$p27^{Kip1}$ induces cell migration. Nat. Med. *4*, 1449–1452.
25. Gius, D.R., Ezhevsky, S.A., Becker-Hapak, M., Nagahara, N., Wei, M.C., and Dowdy, S.F. (1999). Transduced $p16^{INK4a}$ peptides inhibit hypophosphorylation of the retinoblastoma protein and cell cycle progression prior to activation of Cdk2 complexes in late G_1. Cancer Res. *59*, 2577–2580.
26. Schwarze, S.R., Ho, A., Vocero-Akbani, A., and Dowdy, S.F. (1999). In vivo protein transduction: delivery of a biologically active protein into the mouse. Science *285*, 1569–1572.
27. Vocero-Akbani, A.M., Vander-Heyden, N., Lissy, N.A., Ratner, L., and Dowdy, S.F. (1999). Killing HIV-infected cells by transduction with an HIV protease-activated caspase-3 protein. Nat. Med. *5*, 29–33.
28. Lindgren, M., Hällbrink, M., Prochiantz, A., and Langel, U. (2000). Cell-penetrating peptides. Trends Pharmacol. Sci. *21*, 99–103.
29. Wender, P.A., Mitchell, D.J., Pattabiraman, K., Pelkey, E.T., Steinman, L., and Rothbard, J.B. (2000). The design, synthesis, and evaluation of molecules that enable or enhance cellular uptake: Peptoid molecular transporters. Proc. Natl. Acad. Sci. USA *97*, 13003–13008.
30. Futaki, S., Suzuki, T., Ohashi, W., Yagami, T., Tanaka, S., Ueda, K., and Sugiura, Y. (2001). Arginine-rich peptides: An abundant source of membrane-permeable peptides having potential as carriers for intracellular protein delivery. J. Biol. Chem. *276*, 5836–5840.

31. Suzuki, T., Futaki, S., Niwa, M., Tanaka, S., Ueda, K., and Sugiura, Y. (2002). Possible existence of common internalization mechanisms among arginine-rich peptides. J. Biol. Chem. *277*, 2437–2443.
32. Nishida, M., Sugimoto, K., Hara, Y., Mori, E., Morii, T., Kurosaki, T., and Mori, Y. (2003). Amplification of receptor signalling by Ca^{2+} entry-mediated translocation and activation of PLCγ2 in B lyphocytes. EMBO J. *22*, 4677–4688.
33. Kurosaki, T. (2000). Functional dissection of BCR signaling pathways. Curr. Opin. Immunol. *12*, 276–281.
34. Allbritton, N.L., Meyer, T., and Stryer, L. (1992). Range of messenger action of calcium ion and inositol 1,4,5-trisphosphate. Science *258*, 1812–1815.
35. Cheley, S., Gu, L.Q., and Bayley, H. (2002). Stochastic sensing of nanomolar inositol 1,4,5-trisphosphate with an engineered pore. Chem. Biol. *9*, 829–838.
36. Hirose, K., Takeshima, H., and Iino, M. (1999). Fluorescent indicators for inositol 1,4,5-trisphosphate based on bioconjugates of pleckstrin homology domain and fluorescent dyes. Anal. Commun. *36*, 175–177.
37. Kim, Y.H., Park, T.J., Lee, Y.H., Baek, K.J., Suh, P.G., Ryu, S.H., and Kim, K.T. (1999). Phospholipase C-δ_1 is activated by capacitative calcium entry that follows phospholipase C-β activation upon bradykinin stimulation. J. Biol. Chem. *274*, 26127–26134.
38. Khodakhah, K., and Armstrong, C.M. (1997). Inositol trisphosphate and ryanodine receptors share a common functional Ca^{2+} pool in cerebellar Purkinje neurons. Biophys. J. *73*, 3349–3357.
39. Oshannessy, D.J., Brigham-Burke, M., Soneson, K.K., and Hensley, P. (1993). Determination of rate and equilibrium binding constants for macromolecular interactions using surface plasmon resonance: Use of nonlinear least squares analysis methods. Anal. Biochem. *212*, 457–468.
40. Mori, Y., Wakamori, M., Miyakawa, T., Hermosura, M., Hara, Y., Nishida, M., Hirose, K., Mizushima, A., Kurosaki, M., Mori, E., et al. (2002). Transient receptor potential 1 regulates capacitative Ca^{2+} entry and Ca^{2+} release from endoplasmic reticulum in B lymphocytes. J. Exp. Med. *195*, 673–681.
41. Hara, Y., Wakamori, M., Ishii, M., Maeno, E., Nishida, M., Yoshida, T., Yamada, H., Shimizu, S., Mori, E., Kudoh, J., et al. (2002). LTRPC2 Ca^{2+}-permeable channel activated by changes in redox status confers susceptibility to cell death. Mol. Cell *9*, 163–173.